LETTERS

Mitochondrial dysfunction in *Drosophila PINK1* mutants is complemented by *parkin*

Jeehye Park[1,2]*, Sung Bae Lee[1,2]*, Sungkyu Lee[1,2], Yongsung Kim[1,2], Saera Song[1,2], Sunhong Kim[1,2], Eunkyung Bae[3], Jaeseob Kim[2,3], Minho Shong[4], Jin-Man Kim[5] & Jongkyeong Chung[1,2]

Autosomal recessive juvenile parkinsonism (AR-JP) is an early-onset form of Parkinson's disease characterized by motor disturbances and dopaminergic neurodegeneration[1,2]. To address its underlying molecular pathogenesis, we generated and characterized loss-of-function mutants of *Drosophila PTEN-induced putative kinase 1* (*PINK1*)[3], a novel AR-JP-linked gene[4]. Here, we show that *PINK1* mutants exhibit indirect flight muscle and dopaminergic neuronal degeneration accompanied by locomotive defects. Furthermore, transmission electron microscopy analysis and a rescue experiment with *Drosophila Bcl-2* demonstrated that mitochondrial dysfunction accounts for the degenerative changes in all phenotypes of *PINK1* mutants. Notably, we also found that *PINK1* mutants share marked phenotypic similarities with *parkin* mutants. Transgenic expression of Parkin markedly ameliorated all *PINK1* loss-of-function phenotypes, but not vice versa, suggesting that Parkin functions downstream of PINK1. Taken together, our genetic evidence clearly establishes that Parkin and PINK1 act in a common pathway in maintaining mitochondrial integrity and function in both muscles and dopaminergic neurons.

The *Drosophila PINK1* gene (also called CG4523) encodes a polypeptide of 721 amino acids with a molecular mass of about 80 kDa (Fig. 1c and Supplementary Fig. S1a). Similar to human PINK1 (ref. 4), structural analysis of *Drosophila* PINK1 protein also revealed two characteristic motifs: a mitochondrial targeting motif and a serine/threonine kinase domain. The kinase domain exhibited 60% similarity (42% identity) to that of human PINK1. Consistent with the localization of human PINK1 (ref. 4), *Drosophila* PINK1 was also found localized in mitochondria (Supplementary Fig. S1b, c).

First, we observed the expression patterns of *PINK1*, and found that its transcripts are ubiquitously expressed throughout all developmental stages (Supplementary Fig. S1d). Its spatial expression in adults was broadly distributed over all segments, but was particularly higher in the thorax (Supplementary Fig. S1e). To reveal *in vivo* roles of PINK1 in *Drosophila*, we generated *PINK1* loss-of-function mutant flies, $PINK1^{D3}$ and $PINK1^{B9}$, as well as revertants ($PINK1^{RV}$) (Fig. 1a), and these alleles were confirmed by conducting Southern, northern and western blot analyses and genetic analysis with *PINK1* RNA-mediated interference lines (Supplementary Fig. S1f, g, Fig. 1b, c and Supplementary Fig. S2, respectively). *PINK1* mutants were viable and developed to adulthood; however, they displayed shorter longevity (Supplementary Fig. S3a) and complete male sterility due to impaired sperm with swelled nebenkern, a specialized mitochondrial derivative (Fig. 1d). Moreover, at the age of 3 days, about 65% of *PINK1* mutants exhibited a downturned wing phenotype with rigidity, and this percentage slightly increased thereafter (Fig. 1e and Supplementary Fig. S3b). To confirm whether this wing phenotype is caused by loss of PINK1 function, we generated UAS-HA-*PINK1* transgenic lines. When PINK1 expression was induced using the *hs*-GAL4 driver in the *PINK1* mutant background, this wing phenotype was remarkably restored (Fig. 1e and Supplementary Fig. S3b). The discovery of the downturned rigid wing phenotype in *PINK1* mutants led us to search for locomotion defects in these flies. As expected, they showed complete defects in flight ability and slower climbing speed, and these phenotypes were all rescued by PINK1 expression (Fig. 1f and g, respectively).

Furthermore, we found another apparent phenotype in the thoraces of *PINK1* mutants right after eclosion (~85%): thoraces were crushed, particularly in the mid-anterior and anterolateral regions (Fig. 1h, i), and the percentage of flies with this crushed thorax phenotype progressively increased over time (~95% at the age of 30 days, Fig. 1i). Cross-thoracic sections of *PINK1* mutants showed abnormal structure and reduced content of indirect flight muscle (Fig. 2a, top row). In the magnified sections of the mutants, we found disorganized muscle fibres and enlarged mitochondria with highly decreased staining intensity (Fig. 2a, bottom row). Consistently, examination of the indirect flight muscle ultrastructure of *PINK1* mutants revealed irregular arrangement of myofibrils and immensely swollen mitochondria with loss of the outer membrane (Fig. 2b and Supplementary Fig. S3c). Given the reduced muscle content and mitochondrial impairment in the mutants, we then investigated whether apoptosis is apparent in the muscles of *PINK1* mutants by performing a TdT-mediated dUTP nick end labelling (TUNEL) assay. TUNEL signals were ubiquitously detected in the indirect flight muscle of *PINK1* mutants, but not in control flies (Fig. 2c). These *PINK1* mutant phenotypes were all rescued by PINK1 expression (Figs 1i and 2a, c). Collectively, these results demonstrate that loss of *PINK1* induces indirect flight muscle degeneration and mitochondrial impairment.

To confirm further mitochondrial impairment in the muscles (Fig. 2b), we quantified mitochondrial abundance in the mutants. As expected, a marked reduction in the levels of mitochondrial DNA (mtDNA) and protein was observed in *PINK1* mutants when compared to the controls (Fig. 2d and Supplementary Fig. S4a, respectively), and these levels were almost completely restored when PINK1 was expressed back in the mutants (Fig. 2d and Supplementary Fig. S4a). We next conducted an ATP quantification assay with the thoraces of the mutant flies to determine whether altered mitochondrial morphology and amount are correlated with its functional loss. Compared to the control flies, *PINK1* mutants showed a more than twofold reduction in ATP level, and this was markedly restored by PINK1 expression (Fig. 2e). Because substantial

[1]National Creative Research Initiatives Center for Cell Growth Regulation, and [2]Department of Biological Sciences, Korea Advanced Institute of Science and Technology, 373-1 Kusong-Dong, Yusong-Gu, Taejon 305-701, Korea. [3]GenExel, Inc., 373-1 Kusong-Dong, Yusong-Gu, Taejon 305-701, Korea. [4]Department of Internal Medicine, and [5]Department of Pathology, Chungnam National University School of Medicine, 640 Daesa-Dong, Chung-Gu, Taejon 301-721, Korea.
*These authors contributed equally to this work.

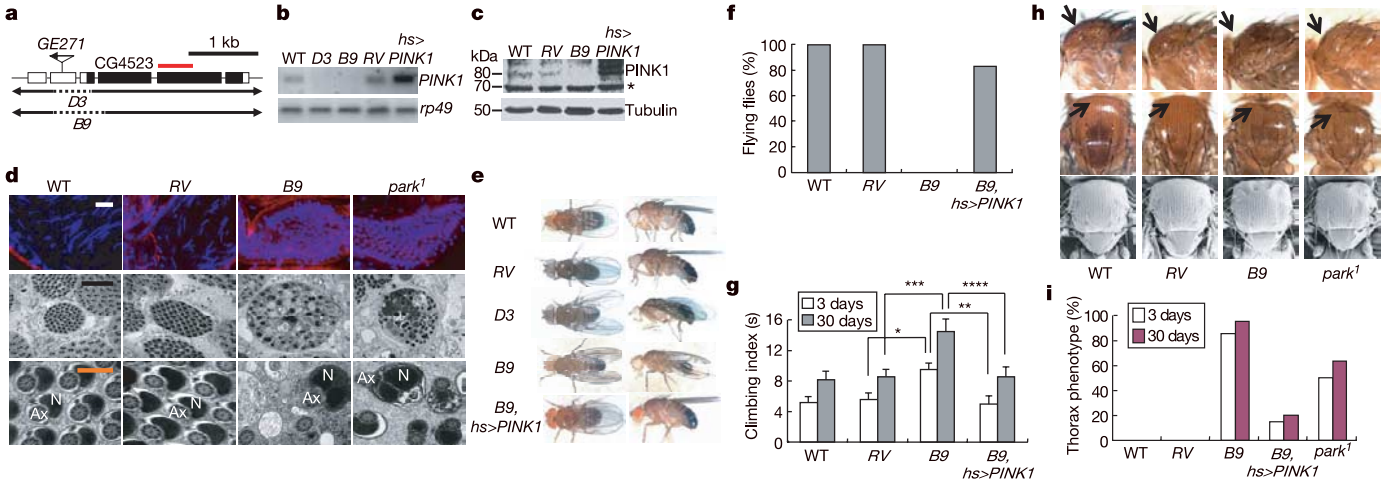

Figure 1 | Characterization of *PINK1* mutants. **a**, Exons of *PINK1* (CG4523) are indicated by boxes, and coding regions are coloured black. The deleted regions for *D3* (*PINK1*^{D3}, 379 bp) and *B9* (*PINK1*^{B9}, 570 bp) are also presented. The red bar indicates the region used as a probe for northern blotting. **b**, **c**, Determination of the expression level of *PINK1* by northern (**b**) and western (**c**) blotting. Asterisk indicates a nonspecific band. **d**, Immunostaining of the nucleus of sperm in 3-day-old male testis (blue, Hoechst 33258; red, α-tubulin; top panels). TEM analysis of spermatozoa from the testis of males hatched within 12 h (middle and bottom panels). Ax, axoneme; N, nebenkern. White scale bar, 5 μm; black scale bar, 5 μm; orange scale bar, 500 nm. **e**, Downturned wing phenotypes of *PINK1* mutants. **f**, Comparison of flight ability. **g**, Comparison of climbing rate (asterisk, $P = 4.59 \times 10^{-4}$; two asterisks, $P = 1.91 \times 10^{-4}$; three asterisks, $P = 1.70 \times 10^{-6}$; four asterisks, $P = 3.46 \times 10^{-5}$). Error bars indicate mean ± s.d. **h**, Collapsed-thorax phenotypes (black arrows) of *PINK1* mutants right after eclosion. **i**, Percentage of collapsed-thorax phenotypes. Details of all the indicated genotypes in this and other figures are described in Supplementary Information.

evidence indicated that anti-apoptotic Bcl-2 families are involved in the protection of mitochondrial integrity and function[5,6], we hypothesized that Bcl-2 expression may suppress the mitochondrial dysfunction and other apparent phenotypes of *PINK1* mutants. As a result, a remarkable recovery of the levels of mtDNA (Fig. 2d), mitochondrial protein (Supplementary Fig. S4a) and ATP (Fig. 2e) was observed after expression of Buffy—a sole *Drosophila* Bcl-2 homologue[7]—under the control of the *hs*-GAL4 driver, whereas its expression in the wild-type background did not affect the mitochondria (Supplementary Fig. S4b–d). Consistently, all of the *PINK1* mutant phenotypes except for the flight defects were markedly restored by Buffy expression (Fig. 2a, f and Supplementary Fig. S4e, f). Overall, these results strongly suggest that mitochondrial dysfunction is the main cause of these aberrant phenotypes of *PINK1* mutants.

Because dopaminergic neurodegeneration is one of the major characteristics of AR-JP patients[2], we examined whether dopaminergic neurons in the brains of adult mutant flies are also impaired. Using immunostaining with tyrosine hydroxylase (TH) antibody, the number of dopaminergic neurons was counted in a blind fashion. For *PINK1* mutants, the number of dopaminergic neurons within each of the major clusters—including dorsomedial (DM), dorsolateral (DL) 1 and 2, and posteriomedial (PM) clusters—was not changed at 3 days (data not shown). However, at 30 days, the mutants exhibited a small but significant decrease (~10%) in the number of dopaminergic neurons in the DM and DL1 regions compared with the wild-type and revertant flies (Fig. 3a, b). This was further confirmed by using another method of expressing nuclear LacZ in dopaminergic neurons (also done in a blind fashion; Supplementary Fig. S5a, b). In

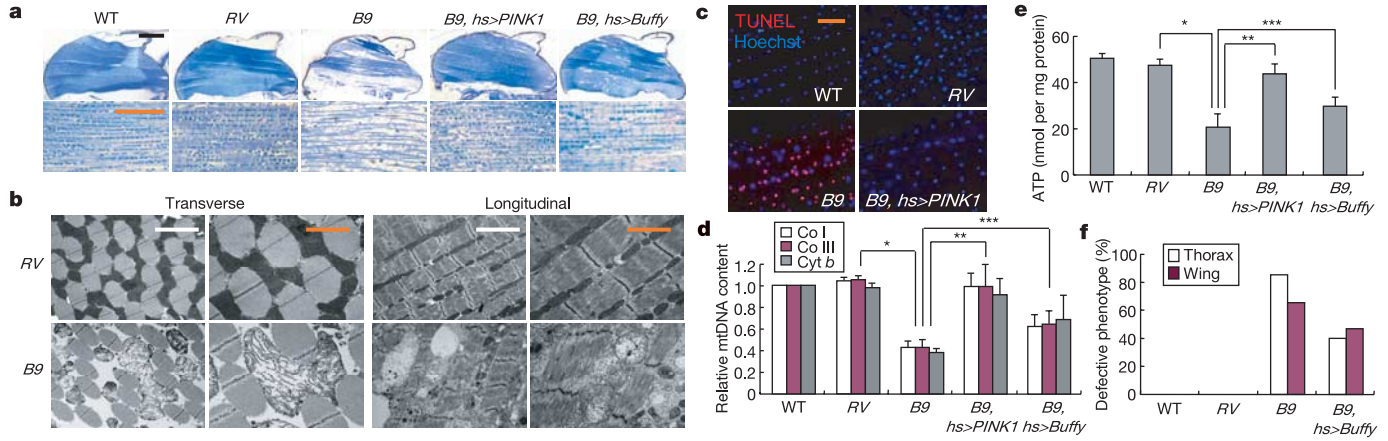

Figure 2 | Mitochondrial defects in *PINK1* mutants. **a**, Longitudinal sections of thoraces. Black scale bar, 200 μm; orange scale bar, 20 μm. **b**, TEM analysis of indirect flight muscle of 2-day-old males. White scale bar, 5 μm; orange scale bar, 2 μm. **c**, Merged images of apoptotic cells (TUNEL, red) and nuclei (Hoechst 33258, blue) of the indirect flight muscle. Scale bar, 20 μm. **d**, Quantification of the mtDNA of thoraces (only the *P* values for cytochrome *c* oxidase subunit III are shown: asterisk, $P = 1.21 \times 10^{-3}$; two asterisks, $P = 9.60 \times 10^{-3}$; three asterisks, $P = 4.47 \times 10^{-2}$; $n = 3$). Co I, cytochrome *c* oxidase subunit I; Co III, cytochrome *c* oxidase subunit III, Cyt B, cytochrome *b*. **e**, Comparison of the ATP content of thoraces (asterisk, $P = 7.20 \times 10^{-4}$; two asterisks, $P = 2.10 \times 10^{-3}$; three asterisks, $P = 3.08 \times 10^{-2}$). **f**, Percentage of defective thorax and wing phenotypes. Error bars in **d**, **e** indicate mean ± s.d.

addition to this neuronal loss at 30 days, the mutants exhibited a markedly decreased anti-TH staining intensity in their dopaminergic neurons (Fig. 3a), which was consistent with their reduced level of dopamine (Fig. 3c). To examine whether the cause of this phenotype is correlated with mitochondrial impairment, we generated *TH>mitoGFP* lines to express mitochondria-targeted green fluorescent protein (GFP) in dopaminergic neurons. In *PINK1* mutants, a number of mitochondria were found to be profoundly enlarged in dopaminergic neurons in all of the clusters, the most severe of which were in the DL1 cluster (Fig. 3d, e and Supplementary Fig. S5c, d), and mitochondrial size progressively increased with age (data not shown). Consistent with this result, transmission electron microscopy (TEM) analysis also revealed grossly enlarged mitochondria in dopaminergic neurons of the mutants (Fig. 3f). In addition, we observed enlarged mitochondria in other neurons, such as surrounding cell bodies of dopaminergic neurons in posterior protocerebrum and neuropils (Supplementary Fig. S6 panels a and b, respectively), and serotonergic neurons (Supplementary Fig. S6d), but not in photoreceptor cells, insulin-secreting cells and circadian pacemaker cells (Supplementary Fig. S6 panels c, e and f, respectively). These results indicate that PINK1 is a critical factor required in dopaminergic neurons for maintaining mitochondrial integrity as well as neuronal function.

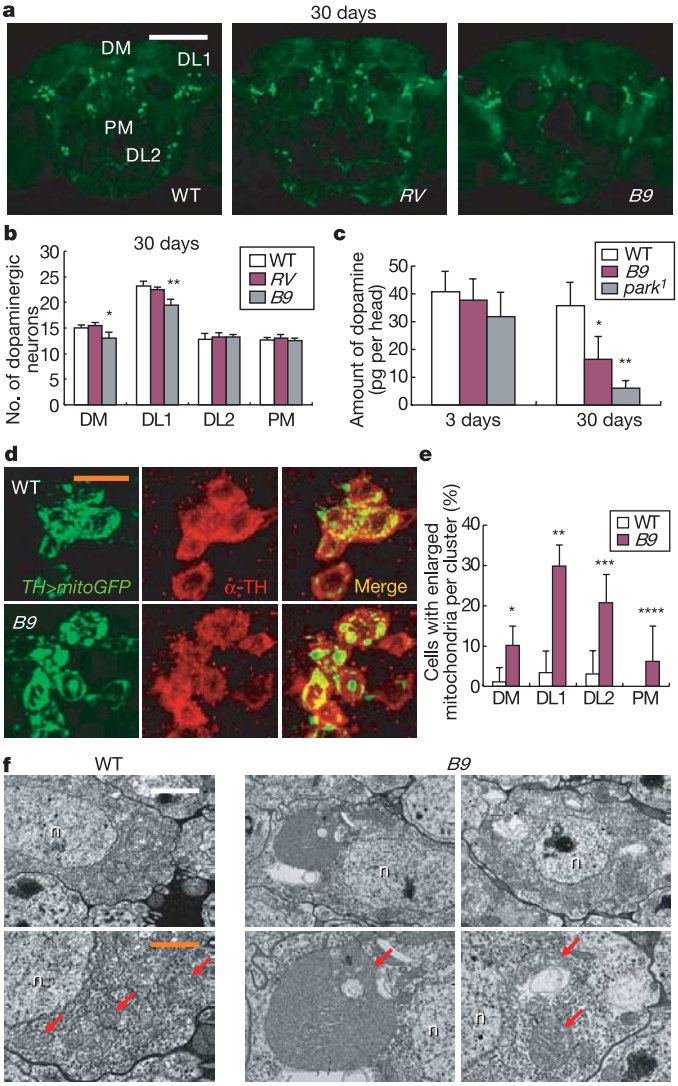

Figure 3 | Dopaminergic neuronal degeneration in *PINK1* mutants. **a**, Whole-mount adult male brains (30-day-old) showing dopaminergic neuron clusters marked by anti-TH antibody (green). Scale bar, 100 μm. **b**, Graph showing the number of dopaminergic neurons in each cluster at 30 days (asterisk, $P = 3.68 \times 10^{-8}$; two asterisks, $P = 2.73 \times 10^{-9}$; $n = 20$). **c**, Amount of dopamine in adult head (asterisk, $P = 6.85 \times 10^{-3}$; two asterisks, $P = 1.19 \times 10^{-3}$; $n = 4$). **d**, Examination of the mitochondria in dopaminergic neurons within the DL1 cluster of 3-day-old adult brain. Scale bar, 10 μm. **e**, Graph showing the percentage of the number of dopaminergic cells with mitochondria larger than 2 μm in diameter over the total number of dopaminergic cells in each cluster (asterisk, $P = 1.13 \times 10^{-5}$; two asterisks, $P = 2.00 \times 10^{-8}$; three asterisks, $P = 9.36 \times 10^{-6}$; four asterisks, $P = 3.83 \times 10^{-2}$; $n = 10$). **f**, TEM analysis of the dopaminergic neurons in the DL1 cluster of 20-day-old adult brain. Red arrows indicate the mitochondria in dopaminergic neurons. n, nucleus. White scale bar, 2 μm; orange scale bar, 1 μm. Error bars in **b**, **c**, **e** indicate mean ± s.d.

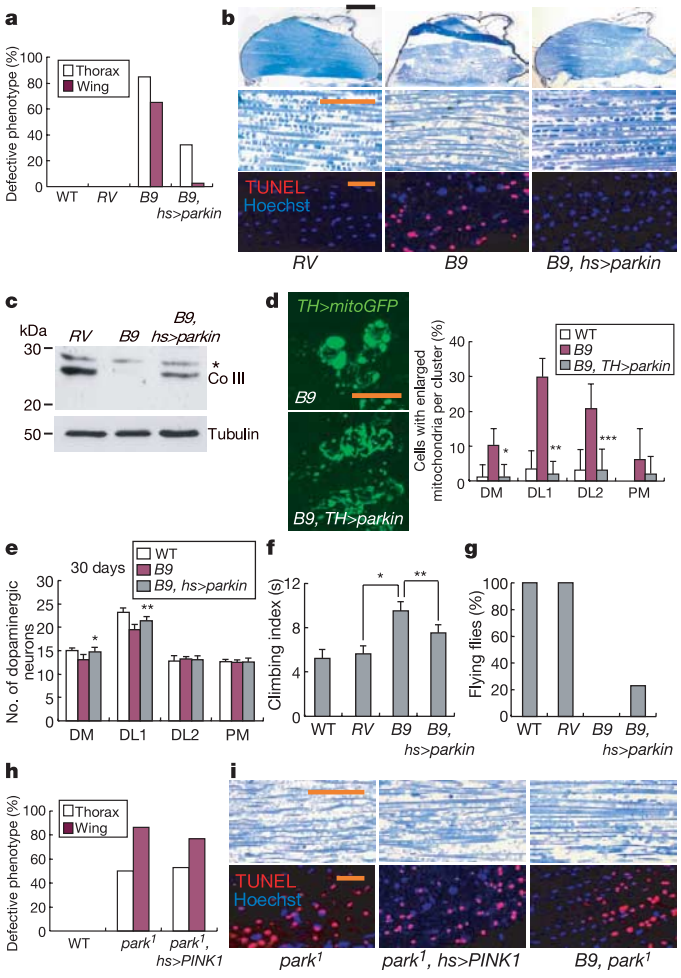

Figure 4 | *In vivo* interaction between PINK1 and Parkin. **a**, Percentage of defective thorax and wing phenotypes. **b**, Longitudinal sections of thoraces (top and middle panels), and merged images (bottom panels) of TUNEL (red) and Hoechst 33258 (blue) staining of the thoraces. Black scale bar, 200 μm; orange scale bar, 20 μm. **c**, Western blot of mitochondrial protein cytochrome *c* oxidase subunit III (Co III) in thoraces ($n = 3$). **d**, Examination of mitochondria in dopaminergic neurons within the DL1 cluster of 3-day-old adult brain (left). Scale bar, 10 μm. Graph showing the percentage of the number of dopaminergic cells with mitochondria larger than 2 μm in diameter over the total number of dopaminergic cells in each cluster (right; asterisk, $P = 5.38 \times 10^{-4}$; two asterisks, $P = 6.32 \times 10^{-10}$; three asterisks, $P = 4.79 \times 10^{-5}$; $n = 10$.) **e**, Graph showing the number of dopaminergic neurons in each cluster at 30 days (asterisk, $P = 3.51 \times 10^{-4}$; two asterisks, $P = 1.04 \times 10^{-5}$; $n = 20$). **f**, Comparison of the climbing rate (asterisk, $P = 4.59 \times 10^{-4}$; two asterisks, $P = 2.40 \times 10^{-2}$). **g**, Comparison of flight ability. **h**, Percentage of defective thorax and wing phenotypes. **i**, Longitudinal sections of thoraces (top panels), and merged images (bottom panels) of TUNEL (red) and Hoechst 33258 (blue) staining of the thoraces. Scale bar, 20 μm. Error bars in **d**–**f** indicate mean ± s.d.

We noticed that all of the phenotypes of the *PINK1* mutants were highly reminiscent of *parkin* mutants generated by other groups and us[8–11]: abnormally positioned wings (Supplementary Fig. S3b), crushed thoraces (Fig. 1h, i), disorganized muscle fibres with enlarged mitochondria (Fig. 4i), muscle cell apoptosis (Fig. 4i), impaired flight ability and highly reduced climbing rate (Supplementary Fig. S8 panels a and b, respectively), complete male sterility due to defective nebenkern (Fig. 1d), and defects in dopaminergic neurons in two particular clusters, DL1 (ref. 10) and DM (refs 8, 9). Therefore, we tested whether there are any possible interactions between these two genes by first expressing Parkin in *PINK1* mutants. The crushed thorax and downturned wing phenotypes of *PINK1* mutants were markedly restored by Parkin expression (Fig. 4a). Muscle sections showed intact structure of muscles and mitochondria in Parkin-expressed *PINK1* mutants (Fig. 4b). Moreover, the mtDNA and mitochondrial protein content as well as the level of ATP in the indirect flight muscle were markedly rescued by Parkin expression (Fig. 4c and Supplementary Fig. S7a, b). Consistent with these findings, TUNEL signals in the indirect flight muscle were almost completely absent (Fig. 4b). In addition, the loss of dopaminergic neurons in the DM and DL1 regions of the *PINK1* mutants was significantly restored by Parkin expression (Fig. 4e), and the enlarged mitochondria in the dopaminergic neurons within the DM, DL1 and DL2 clusters were also markedly rescued (Fig. 4d). Furthermore, the rescued flies showed increased climbing speed and were even able to fly (Fig. 4 panels f and g, respectively). These results indicate that Parkin can compensate for both the mitochondrial dysfunction produced by loss of *PINK1* in muscles and dopaminergic neurons, and for the consequent defective phenotypes. Furthermore, we found that Parkin could not block apoptosis induced by well-known cell death molecules (Supplementary Fig. S7c), suggesting that suppression of PINK1 loss-of-function phenotypes by Parkin expression is not a result of its general protective role against apoptotic insults but rather results from its specific protective role against mitochondrial dysfunction induced by loss of *PINK1*.

Genetic analysis showed that the apparent phenotype as well as the mitochondrial morphology and apoptosis in *parkin* mutants could not be recovered by increased PINK1 expression (Fig. 4h, i and Supplementary Fig. S8a, b). These results indicate that Parkin acts downstream of PINK1 to maintain mitochondrial integrity and function. Moreover, we generated and observed *PINK1* and *parkin* double mutants, and found that they do not show further severity in the phenotype (Fig. 4i and Supplementary Fig. S8c, d) compared to either of the single mutants, implicating that PINK1 and Parkin indeed converge in a common genetic pathway. Furthermore, mitochondrial localization of both of these molecules supports our idea of their functional interaction in that organelle (Supplementary Fig. S8e, f).

We have previously demonstrated that inactivation of the JNK pathway prevents impaired morphology and decreased staining intensity of dopaminergic neurons in *parkin* mutants[8]. Together with the knowledge of the *in vivo* interaction between PINK1 and Parkin, we hypothesized that the JNK pathway may be activated in the indirect flight muscle of *PINK1* mutants. Indeed, using a *puc-lacZ* line (where *puc* is a JNK target gene[12]), we found strong ectopic *puc* expression in the muscles of the *PINK1* mutants, but not in the wild-type flies (Supplementary Fig. S8g). Furthermore, we generated *hep* (a *Drosophila* MKK7 homologue[13]) and *PINK1* double mutants, and found that they show significant restoration of the apparent phenotypes and markedly reduced apoptosis (Supplementary Fig. S8h, i), whereas the mitochondria remain swelled (Supplementary Fig. S8i). Collectively, these data suggest that the mitochondrial impairment-induced apoptosis resulting from *PINK1* ablation is mediated by ectopic activation of the JNK pathway.

Our study provides genetic evidence that PINK1 has a key role in mitochondria, and its dysfunction contributes to the degeneration of high-energy-demanding cells including dopaminergic neurons, muscles, as well as sperm. However, there seems to be some variation in the level of vulnerability to mitochondrial impairment among the tissues and dopaminergic neuron clusters, which might be explained by the different threshold levels for mitochondrial dysfunction-induced cell death among the types of tissues and cells.

All of the phenotypes displayed by *PINK1* mutants were strikingly similar to those of *parkin* mutants. The results of the rescue experiment with the *parkin* transgene provide definitive evidence for the functional interaction between PINK1 and Parkin, and this indicates that Parkin also has a crucial role in maintaining mitochondrial integrity and function. Moreover, through epistatic analysis, Parkin was found to act downstream of PINK1. This finding of the convergence of Parkin and PINK1 in a pathway involved in the protection of mitochondrial integrity provides invaluable clues for understanding the central pathogenic mechanism of AR-JP. Taken together, we anticipate that our *Drosophila* system will be highly useful in future studies, such as investigation into how PINK1 and Parkin protect mitochondrial integrity, and identification of the upstream and downstream molecules involved in this pathway. Our findings will lead to the development of better and effective treatment strategies for AR-JP and possibly other forms of Parkinson's disease, which should be aimed specifically against mitochondrial dysfunction.

METHODS

Fly stocks. From the GenExel library, we isolated a P-element insertion line (*PINK1*^{GE271}) in the second exon of the gene (Fig. 1a). *PINK1*^{D3} and *PINK1*^{B9} alleles were generated through imprecise excision of the P element of *PINK1*^{GE271} and found to be loss-of-function mutants for *PINK1* (Fig. 1b, c). We also generated a revertant allele (*PINK1*^{RV}) by precise excision (but has 40 bp of the P element), which showed almost the same amount of transcript and protein as to that of the wild type (Fig. 1b, c). The generation of *park*^{1} mutants and UAS-*parkin* has been described previously[8]. The UAS-*Buffy* fly line was a gift from H. Richardson[7]; the UAS-*mitoGFP* line was from H. J. Bellen[14] (generated by A. Pilling and W. Saxton). The *TH*-GAL4 fly line was a gift from S. Birman[15]. The *hs*-GAL4 line was obtained from the Bloomington Stock Center.

Northern blotting, mtDNA PCR and immunoblot analysis. Northern blotting was conducted as previously described[16] with purified mRNA using a 504-bp fragment of *PINK1* open reading frame (Fig. 1a) as a probe. For mtDNA PCR, total DNA of thoraces of 2-day-old flies was extracted and subjected to PCR. The genomic DNA level of *rp49* of each sample was also examined by PCR and used as a loading control. Results are expressed as fold change relative to the control. Immunoblot analysis was conducted as previously described[17] with the thoraces of 2-day-old flies. Mouse monoclonal anti-cytochrome *c* oxidase subunit III (yeast) antibody (Molecular Probes), anti-β-tubulin (E7) mouse antibody (Developmental Studies Hybridoma Bank (DSHB)) and rabbit anti-PINK1 antibody were used at 1:1,000 dilutions. The polyclonal antibody to *Drosophila* PINK1 was generated in rabbit by injecting glutathione *S*-transferase (GST)-fused PINK1 (amino acids 480–960) and further purified.

Immunostaining and TUNEL assay. Adult brain and testis were fixed with 4% paraformaldehyde and blocked in Tris-buffered saline with 0.1% Tween 20 (TBST) with 2% bovine serum albumin. The primary antibodies used in this study were: anti-TH rabbit antibody (1:50, Pel-Freez) and anti-α-tubulin mouse antibody (1:100, DSHB). Hoechst 33258 (Sigma) was used to visualize the nucleus of sperm. For adult brains, *Z*-series images (images for ×200 were sectioned at 1-μm intervals, and ×1,000 or ×3,000 at 0.3 μm) were obtained by LSM510 confocal microscope. For the TUNEL assay, apoptosis in the thoraces of 2-day-old flies was detected using the *in situ* cell death detection kit (Roche).

Muscle section and TEM. Muscle sections were carried out as previously described[11], but with some modifications. The samples embedded in Spurr's resin were trimmed and sectioned from the lateral side of the thorax (at a thickness of 5 μm between 150 μm and 300 μm in depth), and the serial sections were then stained with Toluidine blue dye. About ten thoraces of 2-day-old flies were observed for each genotype. The sections were observed at two magnifications (×100 and ×1,000) for light microscopy (Leica). For TEM analysis, samples were prepared as previously described[9].

ATP assay. Five thoraces from 2-day-old flies were dissected and homogenized in 100 μl of 6 M guanidine-HCl in extraction buffer (100 mM Tris and 4 mM EDTA, pH 7.8) to inhibit ATPases[18], followed by fast-freezing in liquid nitrogen and boiling for 3 min. The samples were then centrifuged to collect the supernatant, which was then diluted (1/750) with extraction buffer and mixed

with luminescent solution (Enliten kit, Promega). The luminescence was measured by a luminometer (Berthold Technologies), and the results were compared to the standards. The relative ATP level was then calculated by dividing the luminescence by the total protein concentration, which was determined by the Bradford method. For Bradford assays, samples were diluted (1/30) with extraction buffer. Average ± s.d. is from $n = 3$ experiments.

Dopamine enzyme immunoassay. Dopamine enzyme immunoassay (LDN) was conducted according to the manufacturer's instruction, but fly samples were prepared as follows: 50 fly heads per genotype were dissected and homogenized in PBS with assay buffer (1 M HCl). Then, after adding extract buffer, they were incubated for 20 min and then centrifuged at 13,000 r.p.m. for 30 min. The supernatant was collected and assayed.

Behavioural assays. For the assay of climbing speed, groups of ten 3-day-old males were transferred into 18-cm-long vials and incubated for 1 h at room temperature for environmental acclimatization. After tapping the flies completely down to the bottom, we marked their climbing time at the 15-cm finish line when more than five flies had arrived. Five trials were performed for each group and repeated with four different groups. The average climbing time (±s.d.) was calculated for each genotype. Flight assay was performed as previously described[11] with 3-day-old males ($n > 100$).

Quantification of wing and thorax phenotypes. For quantification, the percentage of defective thorax and wing phenotypes of 3-day-old males was measured ($n > 300$).

Received 2 March; accepted 11 April 2006.
Published online 3 May 2006.

1. Shen, J. & Cookson, M. R. Mitochondria and dopamine: new insights into recessive parkinsonism. *Neuron* **43,** 301–304 (2004).
2. Moore, D. J., West, A. B., Dawson, V. L. & Dawson, T. M. Molecular pathophysiology of Parkinson's disease. *Annu. Rev. Neurosci.* **28,** 57–87 (2005).
3. Unoki, M. & Nakamura, Y. Growth-suppressive effects of BPOZ and EGR2, two genes involved in the PTEN signaling pathway. *Oncogene* **20,** 4457–4465 (2001).
4. Valente, E. M. *et al.* Hereditary early-onset Parkinson's disease caused by mutations in PINK1. *Science* **304,** 1158–1160 (2004).
5. Vander Heiden, M. G., Chandel, N. S., Williamson, E. K., Schumacker, P. T. & Thompson, C. B. Bcl-xL regulates the membrane potential and volume homeostasis of mitochondria. *Cell* **91,** 627–637 (1997).
6. Vander Heiden, M. G. & Thompson, C. B. Bcl-2 proteins: regulators of apoptosis or of mitochondrial homeostasis? *Nature Cell Biol.* **1,** E209–E216 (1999).
7. Quinn, L. *et al.* Buffy, a *Drosophila* Bcl-2 protein, has anti-apoptotic and cell cycle inhibitory functions. *EMBO J.* **22,** 3568–3579 (2003).
8. Cha, G. H. *et al.* Parkin negatively regulates JNK pathway in the dopaminergic neurons of *Drosophila*. *Proc. Natl Acad. Sci. USA* **102,** 10345–10350 (2005).
9. Greene, J. C. *et al.* Mitochondrial pathology and apoptotic muscle degeneration in *Drosophila* parkin mutants. *Proc. Natl Acad. Sci. USA* **100,** 4078–4083 (2003).
10. Whitworth, A. J. *et al.* Increased glutathione S-transferase activity rescues dopaminergic neuron loss in a *Drosophila* model of Parkinson's disease. *Proc. Natl Acad. Sci. USA* **102,** 8024–8029 (2005).
11. Pesah, Y. *et al. Drosophila* parkin mutants have decreased mass and cell size and increased sensitivity to oxygen radical stress. *Development* **131,** 2183–2194 (2004).
12. Adachi-Yamada, T., Fujimura-Kamada, K., Nishida, Y. & Matsumoto, K. Distortion of proximodistal information causes JNK-dependent apoptosis in *Drosophila* wing. *Nature* **400,** 166–169 (1999).
13. Glise, B., Bourbon, H. & Noselli, S. hemipterous encodes a novel *Drosophila* MAP kinase kinase, required for epithelial cell sheet movement. *Cell* **83,** 451–461 (1995).
14. Verstreken, P. *et al.* Synaptic mitochondria are critical for mobilization of reserve pool vesicles at *Drosophila* neuromuscular junctions. *Neuron* **47,** 365–378 (2005).
15. Friggi-Grelin, F. *et al.* Targeted gene expression in *Drosophila* dopaminergic cells using regulatory sequences from tyrosine hydroxylase. *J. Neurobiol.* **54,** 618–627 (2003).
16. Lee, S. B., Park, J., Jung, J. U. & Chung, J. Nef induces apoptosis by activating JNK signaling pathway and inhibits NF-κB-dependent immune responses in *Drosophila*. *J. Cell Sci.* **118,** 1851–1859 (2005).
17. Kim, S., Jee, K., Kim, D., Koh, H. & Chung, J. Cyclic AMP inhibits Akt activity by blocking the membrane localization of PDK1. *J. Biol. Chem.* **276,** 12864–12870 (2001).
18. Schwarze, S. R., Weindruch, R. & Aiken, J. M. Oxidative stress and aging reduce COX I RNA and cytochrome oxidase activity in *Drosophila*. *Free Radic. Biol. Med.* **25,** 740–747 (1998).

Supplementary Information is linked to the online version of the paper at www.nature.com/nature.

Acknowledgements We would like to thank H. Richardson, H. J. Bellen, A. Pilling, W. Saxton, T. Adachi-Yamada, E. N. Olson, S. Birman, S. Noselli, E. J. Rulifson and G. M. Rubin for fly stocks. We appreciate B. Graham for helping us to get the effective anti-TH antibodies. We also thank the Korea Basic Science Institute for the use of SEM and TEM electron microscopes. We also thank members of the Chung laboratory for discussions. J.C. is grateful to J. Blenis for his encouragement.

Author Information Reprints and permissions information is available at npg.nature.com/reprintsandpermissions. The authors declare no competing financial interests. Correspondence and requests for materials should be addressed to J.C. (jchung@kaist.ac.kr).